Structure of *Acinetobacter* Strain ADP1 Protocatechuate 3,4-Dioxygenase at 2.2 Å Resolution: Implications for the Mechanism of an Intradiol Dioxygenase†

Matthew W. Vetting,‡ David A. D'Argenio,§ L. Nicholas Ornston,§ and Douglas H. Ohlendorf*,‡

Center of Metals in Biocatalysis and Department of Biochemistry, Molecular Biology and Biophysics, 6-155 Jackson Hall, 321 Church St. S.E., University of Minnesota Medical School, Minneapolis Minnesota 55455-0347, Department of Molecular, Cellular and Developmental Biology, Yale University, New Haven, Connecticut 06520-8103

Received January 24, 2000; Revised Manuscript Received May 1, 2000

ABSTRACT: The crystal structures of protocatechuate 3,4-dioxygenase from the soil bacteria *Acinetobacter* strain ADP1 (Ac 3,4-PCD) have been determined in space group *I*23 at pH 8.5 and 5.75. In addition, the structures of Ac 3,4-PCD complexed with its substrate 3,4-dihydroxybenzoic acid (PCA), the inhibitor 4-nitrocatechol (4-NC), or cyanide (CN^-) have been solved using native phases. The overall tertiary and quaternary structures of Ac 3,4-PCD are similar to those of the same enzyme from *Pseudomonas putida* [Ohlendorf et al. (1994) *J. Mol. Biol. 244*, 586−608]. At pH 8.5, the catalytic non-heme Fe^{3+} is coordinated by two axial ligands, $Tyr447^{OH}$ (147β) and $His460^{N\epsilon 2}$ (160β), and three equatorial ligands, $Tyr408^{OH}$ (108β), $His462^{N\epsilon 2}$ (162β), and a hydroxide ion (d(Fe−OH) = 1.91 Å) in a distorted bipyramidal geometry. At pH 5.75, difference maps suggest a sulfate binds to the Fe^{3+} in an equatorial position and the hydroxide is shifted [d(Fe−OH) = 2.3 Å] yielding octahedral geometry for the active site Fe^{3+}. This change in ligation geometry is concomitant with a shift in the optical absorbance spectrum of the enzyme from λ_{max} = 450 nm to λ_{max} = 520 nm. Binding of substrate or 4-NC to the Fe^{3+} is bidentate with the axial ligand $Tyr447^{OH}$ (147β) dissociating. The structure of the 4-NC complex supports the view that resonance delocalization of the positive character of the nitrogen prevents substrate activation. The cyanide complex confirms previous work that protocatechuate 3,4-dioxygenases have three coordination sites available for binding by exogenous substrates. A significant conformational change extending away from the active site is seen in all structures when compared to the native enzyme at pH 8.5. This conformational change is discussed in its relevance to enhancing catalysis in protocatechuate 3,4-dioxygenases.

Many man-made aromatic compounds found in pesticides, paints, solvents, and fossil fuels are sources of pollution and present a hazard to human health due to their toxicity and persistence in the environment (*1*). Another significant natural source of aromatic groups is lignin, a compound that gives higher plants their rigidity and the second most abundant biopolymer in the biosphere (*2*). Considerable study has therefore been focused on the metabolic pathways of organisms that can utilize these compounds as a source of carbon and energy. In the mineralization of aromatic compounds soil bacteria and fungi take complex polycyclic aromatic compounds and process them into a limited number of monocyclic compounds (*3*). These compounds then undergo ring cleavage using a dioxygenase to produce aliphatic products that are funneled into the Krebs cycle. The dioxygenase step is the key reaction in aromatic degradation as previous steps are geared toward preparing the compound for cleavage with the placement of appropriate functional groups on the ring (*4, 5*).

Protocatechuate 3,4-dioxygenase [3,4-PCD[1] (EC 1.13.13) (*6*)] catalyzes the aromatic ring fission of protocatechuate (PCA, 3,4-dihydroxybenzoate) with the concomitant incorporation of both atoms of molecular oxygen. Dioxygenases that act on aromatic compounds typically use a non-heme iron as a cofactor and are divided into two classes: the intradiol dioxygenases, which cleave between the two hydroxyls of the substrate and use ferric iron, and the extradiol dioxygenases, which cleave adjacent to one of the two hydroxyls and typically use ferrous iron. The two classes are proposed to have different mechanisms with the extradiol enzymes activating molecular oxygen for attack on substrate (*7*) and the intradiol enzymes activating the substrate for attack by oxygen (*8*). The structure of several extradiol enzymes have been solved:2,3-dihydroxybiphenyl 1,2-dioxygenase (*9*, *10*), catechol 2,3-dioxygenase (*11*), and protocatechuate 4,5-dioxygenase (*12*). Intradiol and extradiol dioxygenases appear to have arisen independently as no sequence or structural homology is apparent between them.

† This work was supported by grants from the National Institute of Health (GM-46436 to D.H.O.), National Institute of Health Biophysics Training grant (GM-07323 to M.W.V.), Army Research Office Grant DAAG55-98-1-0232, and National Science Foundation Grant MCB-9603980 to (L.N.O.).

* To whom correspondence should be addressed. Phone: (612) 624-8436. Fax: (612) 624-5121.

‡ University of Minnesota Medical School.

§ Yale University.

[1] Abbreviations: 3,4-PCD, protocatechuate 3,4-dioxygenase; Ac 3,4-PCD, 3,4-PCD from *Acinetobacter strain* ADP1; Pp 3,4-PCD, 3,4-PCD from *Pseudomonas putida*; Bf 3,4-PCD, 3,4-PCD from *Brevibacterium fuscum*; 1,2-CTD, catechol 1,2-dioxygenase; Ac 1,2-CTD, 1,2-CTD from Acinetobacter strain ADP1; RMS, root-mean-squared; PCA, protocatechuate or 3,4-dihydroxybenzoate; 4-NC, 4-nitrocatechol; INO, 2-hydroxy-isonicotinic acid *N*-oxide; NNO, 6-hydroxy-nicotinic acid *N*-oxide.

10.1021/bi000151e CCC: $19.00
Published on Web 06/17/2000

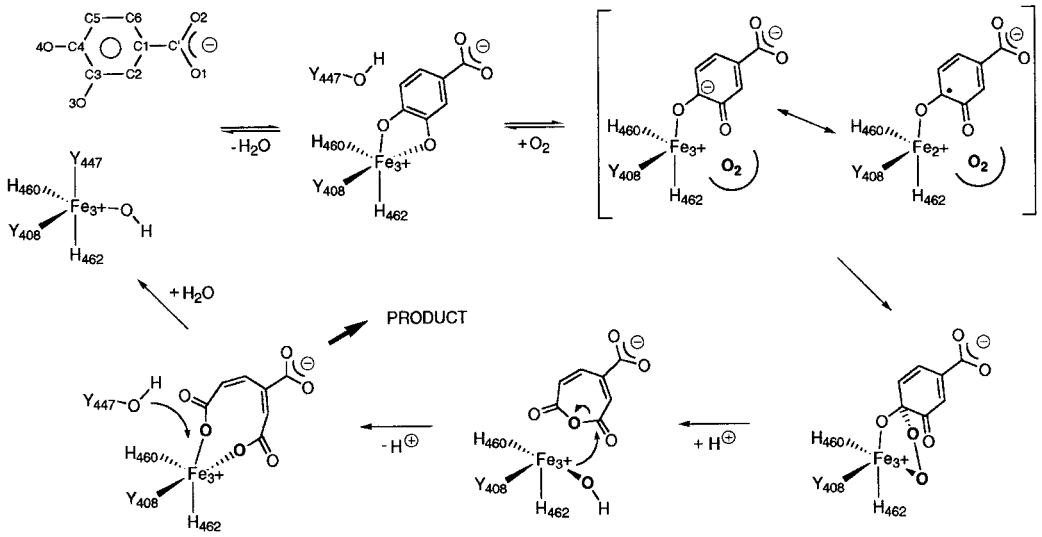

FIGURE 1: Proposed mechanism of 3,4-PCD (adapted from ref *25*).

Intradiol dioxygenases can be subdivided into two subgroups based on sequence alignments and substrate specificity. Catechol 1,2-dioxygenases (1,2-CTDs) cleave catecholate molecules (i.e., catechol, chlorocatechol, dihydroxyquinol) while protocatechuate 3,4-dioxygenases (3,4-PCDs) are specific for dihydroxybenzoate. 3,4-PCD from *Pseudomonas putida* (Pp 3,4-PCD)[2] is the only 3,4-PCD for which a three-dimensional structure has been determined (*13*, *14*). Recently, we solved the structure of catechol 1,2-dioxygenase from *Acinetobacter* strain ADP1 (Ac 1,2-CTD) (*15*). 1,2-CTDs and 3,4-PCDs have catalytic domains with similar folds, but have large differences in accessory domains, and oligomeric structure. The structure of the anaerobic complex of Ac 1,2-CTD with substrate is consistent with earlier biochemical and kinetic data that indicated 1,2-CTDs and 3,4-PCDs have similar mechanisms (*15*−*17*).

3,4-PCD has been purified from a number of organisms and always consists of protomers formed by an equal number of α and β subunits. Each $\alpha\beta$ protomer contains 1 equiv of Fe^{3+}. Different 3,4-PCDs have been observed to have a widely varying number of protomers ranging from $(\alpha\beta Fe^{3+})_2$ for *Agrobacterium radiobacter* (*18*) to $(\alpha\beta Fe^{3+})_{12}$ for Pp 3,4-PCD (for a review, see ref *19*). Several structural studies have been initiated to examine this diversity. The purification and crystallization of recombinant *Acinetobacter* strain ADP1 3,4-PCD (Ac 3,4-PCD) demonstrated that its stoichiometry is also $(\alpha\beta Fe^{3+})_{12}$ (*20*). The utility of using Ac 3,4-PCD as a vehicle to study intradiol dioxygenases is the availability of a growth selection protocol that generates a pool of Ac 3,4-PCD mutants with altered activity (*21*, *22*). In addition *Acinetobacter* strain ADP1 readily undergoes natural transformation (*23*), simplifying manipulation of its genome. The three-dimensional structure of Ac 3,4-PCD is therefore critical to understanding the effects of published (*22*) and future mutants of Ac 3,4-PCD.

An important characteristic of any proposed mechanism for aromatic ring cleaving dioxygenases is that both atoms of molecular oxygen must be retained during the reaction and inserted into product. A combination of kinetic, spectroscopic, and crystallographic data have led to a proposed mechanism for intradiol dioxygenases that is consistent with this requirement (*8*, *24*, *25*). In this mechanism (see Figure 1), the resting state of Fe^{3+} is ligated by two tyrosines, two histidines, and a hydroxide ion in trigonal bipyramidal geometry. The interaction of substrate with Fe^{3+} causes the dissociation of both the axial tyrosine and the hydroxide resulting in a chelated substrate−Fe^{3+} complex that is best described as octahedral with one open coordination site. The interaction of the substrate with Fe^{3+} and molecular oxygen promotes ketonization at O3 yielding a transient carbanion or Fe^{2+}-semiquinone radical. The subsequent reaction with O_2 yields a C4-peroxy intermediate that is coordinated to the Fe^{3+} through the remaining open coordination site. Acyl migration and O−O bond cleavage would yield the cyclic anhydride. The second atom of molecular oxygen is retained at the Fe^{3+} as an oxide or hydroxide ion where it functions as a nucleophile to hydrolyze the anhydride yielding the ring open product.

This mechanism proposes that the ability of substrate to ketonize is a key step in its reaction with oxygen, and is enhanced through the coordination of the substrate to the Fe^{3+} as a dianion. The departing Fe^{3+} ligands are proposed to act as the proton acceptors during the initial binding steps. The binding of 4-nitrocatechol (4-NC) has been used to show the state of ionization of molecules that chelate dioxygenases (*26*, *27*). The visible absorbance spectrum of Pp 3,4-PCD in complex with 4-NC was found to be similar to the dianionic form of 4-NC in solution, suggesting that it binds Pp 3,4-PCD as a dianion. However, despite being isosteric with PCA, 4-NC is not turned over by the enzyme, instead acting as a tight binding ($K_i = 0.9\ \mu M$) competitive inhibitor. The question arises as to why 4-NC is not turned over, even at a slow rate, if the binding modes are the same. We undertook the structure of Ac 3,4-PCD in complex with PCA and 4-NC to determine its mode of inhibition: Is the difference structural (i.e., different binding modes), or is it electronic (i.e., different delocalization states)?

Another important feature of the active site is the utilization of three juxtaposed coordination sites to promote catalysis and assist in the retention of reaction intermediates. The strong affinity of cyanide for Fe^{3+} atoms has been used

[2] American Type Culture Collection (ATCC) 23975 previously classified as *P. aeruginosa*.

Table 1: Data Set Statistics

	native 1	native 2, pH 8.5	native 3, pH 5.75	+PCA, 30 mM	+4-NC, 30 mM	+NaCN, 200 mM
no. of crystals	2	1	1	1	1	1
cell axes (Å)	$a = 145.06$	$a = 145.50$	$a = 144.52$	$a = 144.40$	$a = 144.3$	$a = 144.90$
max resolution (Å)	2.20	2.25	2.25	2.20	2.25	2.15
unique reflections	25,366	23,933	23,288	25,259	23,742	27,540
redundancy	6.3	6.3	5.7	4.3	4.8	4.6
completeness (%)[a]	96.6 (87.1)	98.6 (92.3)	95.8 (80.0)	97.4 (86.4)	98.2 (91.1)	98.2 (90.6)
R_{sym} (%)[a]	9.2 (37.3)	7.4 (32.2)	10.5 (27.6)	9.2 (33.2)	8.9 (32.1)	8.7 (30.5)
$I/\sigma(I)$[a]	6.6 (1.0)	9.0 (1.2)	6.7 (1.0)	6.5 (0.9)	6.5 (1.0)	8.7 (1.0)
refinement statistics						
resolution range (Å)	20−2.2	20−2.25	20−2.25	20−2.2	20−2.25	20−2.15
R/R_{free}	17.9/21.0	17.6/21.8	18.5/22.9	18.2/22.2	17.1/20.9	18.6/24.1
protein atoms ($Z > 1$)	3530	3528	3528	3528	3528	3528
water molecules	178	184	158	194	185	186
ligand atoms	6	1	6	12	12	7
RMSD						
bond length (Å)	0.0060	0.0055	0.0060	0.0058	0.0059	0.0057
bond angles (deg)	1.4	1.5	1.5	1.5	1.5	1.5
average B (Å^2)						
α-subunit	24.56	26.1	25.4	17.5	22.0	20.2
β-subunit	17.9	19.4	17.4	12.6	16.6	14.8
waters	21.5	22.1	19.4	17.2	20.6	19.8
ligand/Fe	57.7/16.0	−/14.7	71.3/15.3	18.7/11.2	33.2/17.5	15.9/12.1

[a] Statistics in parentheses are for highest resolution shell.

as a probe for the type of metal in the active site (*7*, *28*) and the availability of coordination sites for small molecules (*29*, *30*). Biochemical data suggest that 3,4-PCD from *Brevibacterium fuscum* (Bf 3,4-PCD) binds two to three cyanides in a two-step process, and that intradiol dioxygenases have three coordination sites that are available to exogenous ligands (*31*). The determination of the X-ray structure of Ac 3,4-PCD with cyanide clarifies the number of sites competent to bind cyanide and yields insight into the nature of those coordination sites.

In this report, we describe the structures of Ac 3,4-PCD at pH 8.5 and at pH 5.75 and of complexes of Ac 3,4-PCD with PCA, 4-NC, or cyanide. Comparisons of these structures with Pp 3,4-PCD and its complexes (*25*, *32*) give insight into the structure/function relationship of intradiol dioxygenases.

MATERIALS AND METHODS

Crystallization. The expression, purification, and crystallization of recombinant Ac 3,4-PCD have been described in detail elsewhere (*20*). Briefly, crystals of purified Ac 3,4-PCD were grown at 18 °C using the hanging drop method with 1.8 M ammonium sulfate, 50 mM Tris-HCl, pH 7.0, in the reservoir and 10 mg/mL protein in the drop. The crystals grew as perfect dodecahedrons and had a typical diameter of 0.2−0.3 mm. Macrocrystal seeding was used to increase the dimensions of the crystals to >0.5 mm with a concomitant increase in resolution from about 2.6 Å to better than 2.2 Å. The space group of these crystals was $I23$ with $a = 145$ Å (see Table 1).

A second crystal form was observed in the same drops in which the $I23$ form was found, although it was more prevalent in drops with slightly lower pH. These crystals belonged to the space group $P2_13$ with $a = 192$ Å. The $P2_13$ crystal form typically grew faster, was twice to three times larger in size, and had a similar yet identifiable morphology compared to the $I23$ form. Seeding with small crystals of the $I23$ form produced hanging drops which only contained $I23$ crystals, allowing the growth of larger $I23$ crystals. The $P2_13$ crystal form was not pursued due to the number of protomers in the asymmetric unit (four compared to one), the lower observed resolution (2.8 Å), and the difficulty in collecting diffraction data from crystals having such a long unit cell axis.

An initial data set for the $I23$ crystal form was collected using two crystals, each mounted using the reservoir solution as a mother liquor (pH ∼7). These data sets were merged (native 1) and used to determine the molecular replacement solution and the first refined structure. To ensure that any differences between Ac 3,4-PCD and Pp 3,4-PCD were not due to a pH difference, two separate data sets (native 2 and native 3) were collected from crystals that were incubated in a mother liquor containing either 100 mM Tris-HCl, pH 8.5, or 100 mM sodium cacodylate, pH 5.75 (see Table 1). The diffraction data for the complexes were collected on crystals soaked for 1 h in a mother liquor containing 100 mM Tris-HCl, pH 8.5, and 30 mM, 30 mM, or 200 mM of PCA, 4-NC, or NaCN, respectively. For the PCA and 4-NC complexes, soaks and crystal mounting were performed in an anaerobic glovebox and the capillaries were sealed with mineral oil and epoxy to exclude oxygen.

Intensity data were collected at room temperature on a Siemens-Nicolet 100 area detector. Monochromatic CuKα radiation was produced by a Rigaku RU-200 rotating anode generator operating at 45 kV, 200 mA with a 0.5 X 10 mm focal spot. The data were processed and scaled using the XENGEN software package (*33*). The resolution cutoff was defined by where I/σ_I fell to 1.0. The data collection statistics are summarized in Table 1. In all data sets 5% of the measured reflections were set aside and used to calculate *R*-free (*34*).

An added caveat to the purification and crystallization of Ac 3,4-PCD is the ability to add back Fe^{3+} to the enzyme to get a full complement of active sites. The active sites of Ac 3,4-PCD and Pp 3,4-PCD when purified from the native organisms are only 50−70% occupied with Fe^{3+} (*35*, *36*).

When Ac 3,4-PCD or Pp 3,4-PCD is overexpressed in *Escherichia coli*, this percentage drops to less than 30% (data not shown). The low Fe^{3+} occupancy explains the low specific activity of Ac 3,4-PCD seen in the crude extract of the recombinant clone despite being overexpressed (*37*). Using the reconstitution technique of Fujiwara and Nozaki (*38*), we are able to obtain active sites with full occupancy (11−12 Fe^{3+}/molecule). This reconstitution procedure ensures that the interpretation of the native structure and small molecule complexes are not tainted by active sites without Fe^{3+}.

Structure Determination and Refinement.. The structure of unliganded Ac 3,4-PCD was determined by molecular replacement using a single protomer of the 2.15 Å structure of Pp 3,4-PCD (*14*) as the search model. Amino acids that were not conserved in both Ac 3,4-PCD and Pp 3,4-PCD were changed to alanines to minimize model bias. All molecular replacement solutions were obtained using the program X-PLOR (39) and data between 15 and 4 Å. Using a Patterson cutoff radius of 40 Å, a list of 100 rotation function peaks were obtained, with the top peak being 3.6σ above the mean. The translation function gave an unambiguous solution that was 7.3σ above the next highest peak. The model output from molecular replacement was subjected to rigid-body refinement and underwent several rounds of manual rebuilding, simulated annealing and conventional positional and thermal parameter refinement. All model building was carried out using the program O (*40*), and all crystallographic refinements were performed using CNS (*41*). After each round of refinement, side chains were added to the model where electron density maps supported their placement. Water molecules were added when they met three criteria: (1) there were peaks in the $|F_o| - |F_c|$ maps higher than 4σ, (2) there were matching peaks in the $2|F_o| - |F_c|$ map at 1σ, and (3) and they were within hydrogen-bonding distance from appropriate atoms. In the refinement of other data sets, the starting model was that obtained for native 1 after removal of all nonprotein atoms. One round of rigid body refinement and torsional dynamics simulated annealing at 5000 K was performed to minimize model bias. The van der Waals interaction energy was turned off for all ligands to the Fe^{3+} so that the refinement of ligand to metal distances was driven purely by the electron density. In cases where the location of Tyr447[3] was in question, it was first refined as a serine. In all cases, exogenous ligands to the Fe^{3+} were not included until the last round of refinement.

Native Data at Varying pH. In the initial refinements of native 1 and native 3, a large positive difference peak in an equatorial position opposite Tyr408 remained after all protein atoms were included in the model. Positional refinement by CNS with refinement of the thermal and occupancy parameters was used to determine that a sulfate ion best fit the electron density. In all the native data sets $2|F_o| - |F_c|$ density and $|F_o| - |F_c|$ positive difference density was found opposite His460, which was subsequently modeled as a water. Examination of $|F_o^{pH8.5}| - |F_o^{pH5.75}|$ maps revealed a cascade of features that originate from the active site and propagate through the $\alpha\beta$ subunit interface to the surface. Simulated annealing refinement of the Ac 3,4-PCD structure at pH 5.75 resulted in an alternate conformation for several residues in this interface region. No significant manual intervention was used in the interpretation of the electron density in this region. All of the other structures (complexes or native at lower pH) refined in a similar manner resulted in this different conformation. In all cases simulated annealing omit maps confirmed the conformation of residues in this area.

PCA and 4-NC Complex. Phases from the pH 8.5 model were used to make initial $|F_o^{complex}| - |F_o^{native}|$ maps which showed +6σ density opposite Tyr408 and −6σ density over the axial ligand Tyr447. Initial refinement produced clear density for the aromatic compound and for the new position of Tyr447. Refinement after placing PCA in the active site yielded featureless $|F_o| - |F_c|$ maps at this position. To minimize the possibility of model bias PCA was modeled and refined in several orientations. One model invariably produced cleaner difference maps and agreed best with the $2|F_o| - |F_c|$ maps. A similar procedure was used to refine the 4-NC complex.

Cyanide Complex. $|F_o| - |F_c|$ maps after simulated annealing showed three positive difference features continuous with the Fe^{3+}, one of which was near Tyr447. There were negative difference features overlaying a portion of Tyr447 indicating it had dissociated from the Fe^{3+}. Positional refinement of a model that included the Fe^{3+} atom and Tyr447 in a rotated position could not account for the three positive peaks in the coordination sphere of the Fe^{3+}. Since the resolution of the data was not sufficient to distinguish between a water molecule or CN^-, two different starting models were refined against the diffraction data: (1) three water molecules at 2.6 Å from the Fe^{3+} or (2) three CN^-s [d(Fe−CN = 1.9 Å] with linear Fe−C−N geometry and no restraints.

Accession Numbers. The atom coordinates for Ac 3,4-PCD at pH 8.5, pH <7.0, and in complex with PCA, 4-NC or CN^- have been deposited in the Protein Data Bank with accession numbers 1EO2, 1EO9, 1EOB, 1EOC, and 1EOA, respectively.

RESULTS

Structure of Ac 3,4-PCD. Ac 3,4-PCD is a dodecameric enzyme in which protomers are related to each other by *23-(T)* point group symmetry. All of the symmetry elements in this point group are shared by those of the crystallographic space group resulting in a single ($\alpha\beta Fe^{3+}$) protomer per asymmetric unit. This is in contrast to Pp 3,4-PCD, which was solved in a lower symmetry space group (*C*2), and had six ($\alpha\beta Fe^{3+}$) protomers per asymmetric unit (*13*). The high symmetry of the Ac 3,4-PCD crystals leads to a drastic reduction in the time required for data collection and the number of atoms which need to be modeled (one-sixth). This is important for future studies where the analysis of Ac 3,4-PCD mutants requires several three-dimensional structures to be solved.

[3] The numbering of Ac 3,4-PCD is based on the numbering system of Pp 3,4-PCD and sequence alignments between the two proteins. The α subunit is numbered 1−200, while the β subunit is numbered 301 to 540. At points in the sequence where Ac 3,4-PCD does not have a corresponding residue in Pp 3,4-PCD (insertions) these residues are labeled with the original sequence number with sequential lettering (e.g., 1A, 1B, 1C, 1, 2, 3, 3A, 3B, 3D, 4). The Fe+3 is numbered 600. The water (or hydroxyl) bound to the Fe^{3+} is labeled 700. Sulfate, PCA, and 4-NC are labeled 999 while the 3 CN^- are labeled 901−903.

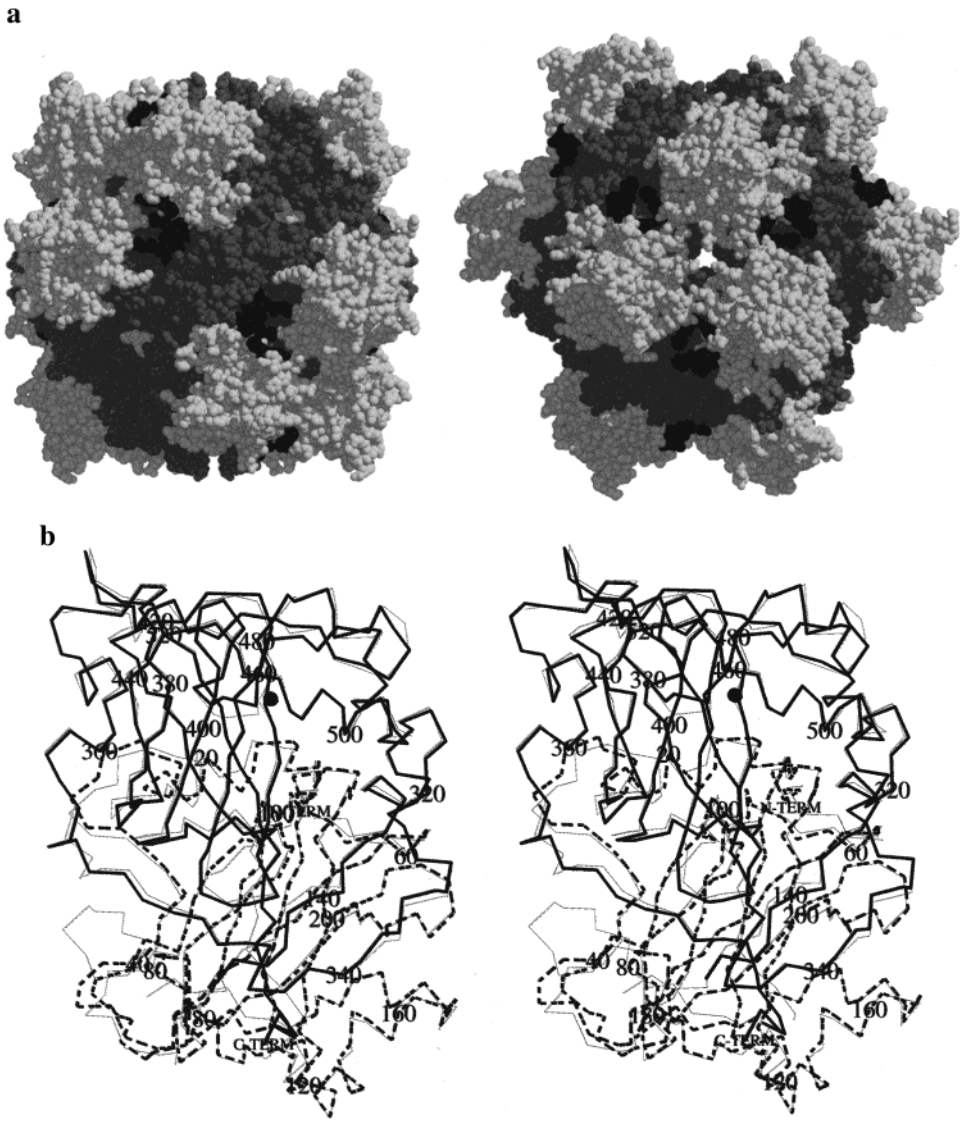

FIGURE 2: (a) Space filling model of the Ac 3,4-PCD aggregate looking down a 2- and 3-fold axis of symmetry, respectively. The 12 α subunits are shown as light gray spheres, while the 12 β subunits are shown as dark gray spheres. Residues which line the twelve active sites are shown as black spheres. (b) Stereoview of the superposition of Cα traces of Ac 3,4-PCD and Pp 3,4-PCD. Ac 3,4-PCD α subunit (thick dotted line), Ac 3,4-PCD β subunit (thick solid line), Ac 3,4-PCD Fe^{3+} ion (black sphere), and Pp 3,4-PCD αβ protomer (thin line). This figure was produced using the program MOLSCRIPT (*62*).

The enzyme has a tetrahedral shape with a diameter ranging from 160 to 125 Å and a 45 Å diameter central cavity (see Figure 2a). The α subunits cluster around the 3-fold symmetry axes and form the apexes of the tetrahedron. The central cavity is accessible to solvent through roughly triangular channels along the 3-folds ranging from 26 to 8 Å on a side. The electrostatic potential surface produced by the aggregate looks very similar to that produced by Pp 3,4-PCD with the most prominent feature consisting of large lobes of negative electrostatic potential radiating from the surface of the α subunits. The large overall negative charge of the molecule (−84 with −7 per protomer) would seem contrary to the binding of a negatively charged molecule such as PCA. It has become a common feature in proteins that have charged substrates that electrostatic interactions, even over long ranges, can be used to guide a substrate to, and or between, active sites (*42*, *43*). A number of basic residues line the entrance to the active site of Ac 3,4-PCD producing these regions of positive electrostatic potential. Many of these residues are solvent exposed, have no compensating negative charges nearby, and serve no apparent structural role. Some are conserved as basic residues in all known 3,4-PCD sequences to date (Arg133, Arg167, Lys325, Arg330, Arg408, and Arg457), while others (Arg64, Arg409, Arg450, and Lys154) are conserved between Pp 3,4-PCD and Ac 3,4-PCD but not necessarily in other species. A comparison of the molecular surfaces of 3,4-PCDs and Ac 1,2-CTD demonstrates that, with the exception of Arg457, most basic residues are not conserved (*15*). This is consistent with the fact that the substrates of 1,2-CTDs are hydrophobic and lends credence to the hypothesis that 3,4-PCDs may use these basic residues to funnel PCA into the active site (*32*).

Each protomer has a cylindrical shape (diameter = 35 Å, length = 60 Å) and is in contact with five other protomers in the molecular aggregate. These interactions are identical for each protomer so discussion can be limited to one protomer. The Ac 3,4-PCD protomer consists of two nonidentical subunits (α and β) associated with one non-heme ferric iron (see Figure 2b). Both subunits have similar folds. The core of each subunit consists of two four-strand

Table 2: Bond Lengths and Angles

	NAT1	NAT2	NAT3	PCA	4-NC	CN
bond lengths (Å)						
Fe−O(408)	1.8	2.1	1.9	1.9	2.0	1.9
Fe−O(447)	2.1	1.9	2.0			
Fe−NE2(460)	2.2	2.2	2.3	2.2	2.3	2.2
Fe−NE2(462)	2.2	2.1	2.1	2.2	2.1	2.1
Fe−site A	1.8 (SO1)		1.9 (SO1)	2.1 (OC3)	2.2 (OC3)	1.9 (CN)
Fe−site B	2.3 (OH)	1.9 (OH)	2.3 (OH)		2.2	2.0 (CN)
Fe−site C				2.1 (OC4)	2.0 (OC4)	1.9 (CN)
bond angles (deg)						
O(408)−Fe-O(447)	100	109	105			
O(408)−Fe-NE2(460)	97	103	101	92	90	87
O(408)−Fe-NE2(462)	91	87	85	97	101	93
O(408)−Fe-site A	167		163	170	174	174
O(408)−Fe-site B	92	113	96		89	94
O(408)−Fe-site C	-			98	100	111
O(447)−Fe-NE2(460)	95	92	95			
O(447)−Fe-NE2(462)	169	163	169			
O(447)−Fe-site A	80		87			
O(447)−Fe-site B	86	89	92			
O(447)−Fe-site C						
NE2(460)-Fe−NE2(462)	84	83	81	91	88	89
NE2(460)-Fe−site A	96		89	98	90	89
NE2(460)-Fe−site B	171	142	159		173	176
NE2(460)-Fe−site C				100	94	96
NE2(462)-Fe−site A	90		83	80	82	92
NE2(462)-Fe−site B	93	85	88		96	95
NE2(462)-Fe−site C				161	159	174
site A- Fe−SITE B	76		72		96	90
site A-Fe−SITE C				80	77	84
site B−Fe−SITE C					83	80

β sheets that fold upon each other to form a β sandwich. One β sheet consists of antiparallel strands, while the other has a mixed topology. Surrounding the core structure is a series of small helices and large irregular loops. The two β sheets form part of the interface between the subunits, with the surrounding loops providing the remaining contacts.

An interesting feature of this interface is the amino terminus of the α subunit, which passes completely through a gap between the core β sandwich and supporting structures of the β subunit to make up one wall of the active-site cavity. A superposition of 152 topologically equivalent C^{α} atoms between the α and β subunits of Ac 3,4-PCD yields an RMS difference of 1.38 Å. A similar alignment between the α and β subunit of Pp 3,4-PCD subunits yields an RMS difference of 1.06 Å (127 residues) (*14*). Despite the high degree of structural similarity, the primary sequences of the α and β subunits have diverged extensively as the subunits of Ac 3,4-PCD and Pp 3,4-PCD have only 26% and 30% sequence identity, respectively.

A primary sequence alignment of Pp 3,4-PCD (*44*−*46*) and Ac 3,4-PCD (*47*) yields a sequence identity of 49% for the α chain and 56% for the β chain with few insertions or deletions. Accordingly, the structure of the protomer of Ac 3,4-PCD is very similar to that of Pp 3,4-PCD (see Figure 2b). The overall RMS deviation for 415 (out of approximately 449) homologous C^{α}s in Pp 3,4-PCD and Ac 3,4-PCD (pH 8.5) is 0.91 Å. All of the large differences in C^{α} positions (>1 Å) are located away from the active site and involve residues on one side of the protomer. This region is largely composed of residues in the α subunit that are exposed to solvent.

Active Site of Ac 3,4-PCD at pH 8.5 (Native 2). All of the ligands to the Fe^{3+} are provided by the β subunit. Two histidines (His460 and His462) and two tyrosines (Tyr408 and Tyr447) ligate the Fe^{3+} in a trigonal bipyramidal geometry significantly distorted toward octahedral with two nonprotein ligand sites (see Table 2). Using the labeling convention for Fe^{3+} ligands in Pp 3,4-PCD, $Tyr447^{OH}$ and $His462^{N\epsilon 2}$ are the axial ligands whereas $Tyr408^{OH}$ and $His460^{N\epsilon 2}$ are the equatorial ligands. The two nonprotein ligand sites are in equatorial positions, one opposite $Tyr408^{OH}$ (site A) and the other opposite $His460^{N\epsilon 2}$ (site B). A third nonprotein ligand site becomes available during the reaction upon dissociation of $Tyr447^{OH}$ from the Fe^{3+} (site C). Substrates and other small molecules have direct access to the catalytic metal through a funnel-shaped channel created by the interaction of three protomers. At the surface, this opening is rectangular with dimensions of approximately 18 Å × 10 Å. Residues Arg64, Asn412, Gln414, and Ile416 project from one side of the opening, while a related protomer donates Lys118′, Lys154′, Val156′, Asn159′, and Arg167′ to create the other side of the rectangular crevice. Further within the funnel, residues Asp65, Phe99, Arg133, Thr326, Asn413, Tyr415, Pro448, and the backbone nitrogen of Arg450 narrow the dimensions to 8 × 10 Å. Finally upon binding the Fe^{3+} atom, substrates interact with Thr12, Pro15, Tyr16, Tyr324, Tyr447, Trp449, Arg457, and Ile491 in a 5 × 7 Å cavity. Several ordered waters fill the planar cavity and appear to solvate residues within the active site when substrate is not bound. A similar water network is present in Pp 3,4-PCD.

The density suggests that at pH 8.5 a solvent molecule (WAT700) binds to the Fe^{3+} in the equatorial plane (see Figure 3a). This is consistent with EPR experiments which show hyperfine broadening of the $g_z = 9.67$ and $g_{xyz} = 4.28$ signal upon incubation of Bf 3,4-PCD with $H_2{}^{17}O$ (*29*). This

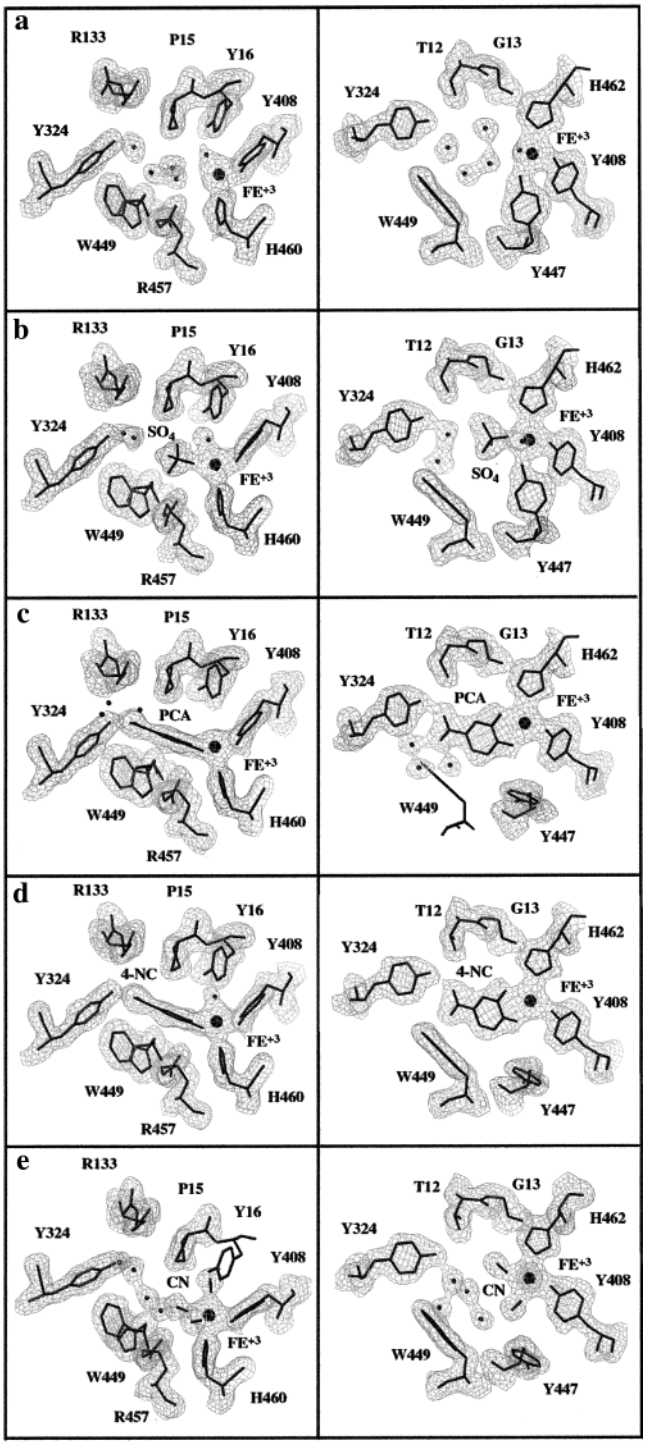

FIGURE 3: $2|F_o| - |F_c|$ maps of active sites of (a) Ac 3,4-PCD at pH 8.5, (b) Ac 3,4-PCD at pH 5.75, (c) Ac 3,4-PCD complex with PCA, (d) Ac 3,4-PCD complex with 4-NC, and (e) Ac 3,4-PCD complex with cyanide. The related figures are 90° rotations of a, b, c, d, and e about the *x*-axis. The density for Tyr16 and Trp449 is not shown in some figures to permit the display of other density features in the active site. This figure was prepared using the program O (*63*).

solvent, also seen in the native Pp 3,4-PCD structure, is proposed to be a hydroxide ion because of the short bond distance to the Fe^{3+} [d(Fe−O) ∼1.9 Å].

Active Site of Ac 3,4-PCD at pH 5.75. Structural models produced from native 1 (pH ∼5−7) and native 3 (pH 5.75) indicate that a sulfate ion becomes a ligand to the Fe^{3+} as the pH is lowered below 7 (see Figure 3b). The sulfate binds

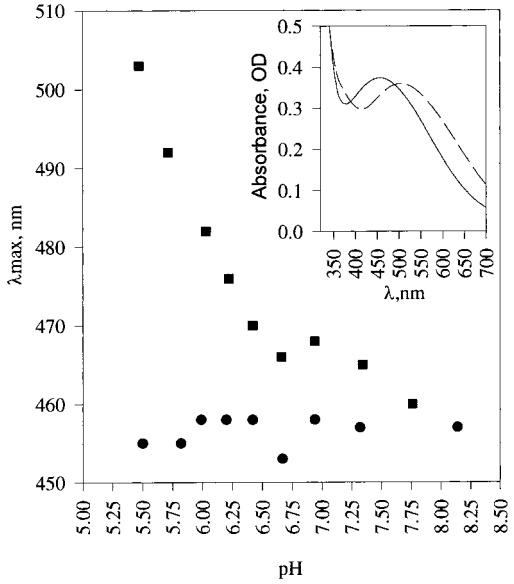

FIGURE 4: Shift in λ_{max} as a function of pH for Ac 3,4-PCD with (squares) and without 1.5 M ammonium sulfate (circles). (Inset) Spectrum of Ac 3,4-PCD at pH 7.0 with (dashed) and without 1.5 M ammonium sulfate (solid).

trans to Tyr408, with its −2 charge neutralized by the Fe^{3+} and Arg457. In this model, the distance between WAT700 and the Fe^{3+} is lengthened to 2.3 Å, suggesting that the bound hydroxide has been protonated. Figure 4 shows that sulfate causes a significant shift in the absorption spectrum of Ac 3,4-PCD from $\lambda_{max} = 458$ nm to $\lambda_{max} > 500$ nm as the pH is shifted from 8 to 5.5. The change can be ascribed to the sulfate alone as a pH change without ammonium sulfate in the conditions produces no shift in the optical maximum. A similar shift in the optical spectrum has been seen in the complex of Pp 3,4-PCD with the product analogues terephthalate and glutarate (*48*).

There is a significant shift in the positions of several residues near the active site that propagates along the $\alpha\beta$ interface and out to solvent. The change is more apparent in several other structures presented here and will be discussed later.

PCA Complex. The density suggests the substrate is bound to the Fe^{3+} in a symmetric bidentate mode displacing the bound hydroxide and four solvent molecules (see Figure 3c). The mean thermal parameter for the substrate is 18.7 $Å^2$, indicating it is well ordered and has high occupancy. Using $Asp65^{C\beta}$, $Arg133^{N\epsilon1}$, $Asn413^{O}$, $Pro448^{O}$, and $Arg450^{O}$ to define the mouth of the inner substrate binding cavity, the solvent-accessible volume is 225 $Å^3$ when PCA is bound (see Figure 5). The planar shape of this cavity suggests that the active site promotes the binding of the aromatic ring of PCA in the axial plane. In this binding mode, PCA^{O3} occupies the equatorial position opposite $Tyr408^{OH}$ and PCA^{O4} occupies the axial position opposite $His460^{N\epsilon2}$ with nearly equivalent bond distances of approximately 2.1 Å (see Figure 1 for PCA atom label convention). The axial binding of the C4 hydroxyl leads to the dissociation of Tyr447 from the Fe^{3+} through a rotation around the C2 carbon converting Tyr447 from one common rotamer to another (gauche$^-$ to trans). Tyr447 rotates into a portion of the active-site pocket formed by Arg407, Tyr408, Asp413, Tyr415, and Pro448 resulting in the dissociation of two water molecules. Single

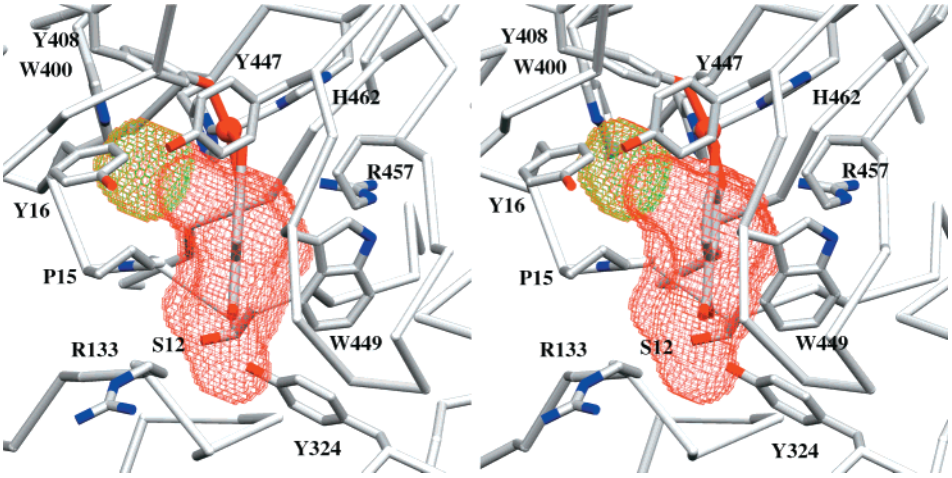

FIGURE 5: Divergent stereoview of the free volume in the active-site cavity before (red wire) and after binding PCA (green wire) superimposed on the Ac 3,4-PCD PCA complex structure. Fe^{3+} is shown as a red sphere ligated to three protein ligands and the two hydroxyls of substrate. Wire volume calculated using the program VOIDOO (*64*). Figures 5 and 6 were prepared using the program SETOR (*65*).

turnover kinetics of a Tyr447 to histidine mutant in Pp 3,4-PCD indicates that Tyr447 is critical to both the binding of substrate, and dissociation of product (*49*). In its new position $Tyr447^{OH}$ forms favorable interactions through hydrogen bonds with $Tyr16^{OH}$ and $Asp413^{O\epsilon1}$ that are offset by unfavorably burying two potential hydrogen bonds ($Gly406^{O}$ and $Pro448^{O}$). The balance of these two interactions ensures that Tyr447 is stable in this rotated conformation when Fe^{3+} is interacting with substrate but is able to rebind to the Fe^{3+} after product forms.

Other residues in the cavity appear to be crucial in the positioning of PCA. Two residues constrict the active site cavity on either side of the plane of PCA. Pro16 protrudes into the active-site cavity and interacts with the middle of the aromatic ring. On the opposite side, Arg457 makes a 2.8 Å contact with the C3 hydroxyl of PCA and is no longer solvent accessible upon binding the substrate. Arg457 has been proposed to stabilize the carbanion character of the C4 carbon through electrostatics and is conserved in all known intradiol dioxygenases (*14*, *25*). Mutation of Arg457 to a serine in Ac 3,4-PCD resulted in an *Acinetobacter* strain unable to grown on 4-hydroxybenzoate (*21*). Trp449 and Ile491 interact with C6 and C2 of the aromatic ring on the same side as Arg457. The Cβ, Cγ, and Cδ of Arg133 interact with C′ of the substrate on the same side as Pro16. The carboxyl group of PCA forms a hydrogen bond ($d = 2.5$ Å) to Tyr324, and its negative charge is complemented by long-range electrostatic interactions with Arg133, Arg330, and Arg450. The binding of PCA in such an orientation, with the rotation of Tyr447, fills almost all of the substrate binding cavity near the Fe^{3+}.

The remaining volume near the Fe^{3+} that is not occupied by PCA is the most likely position from which oxygen interacts with substrate. This cavity is opposite His460 and is formed by residues Gly13, Gly14, Pro15, Tyr16, Val17, Trp400, Tyr408, His462, and the Fe^{3+} atom (see Figure 5). The binding of PCA does not alter the shape of this 32 $Å^3$ cavity; however, it is no longer accessible to solvent. A superposition of Pp 3,4-PCD, Ac 3,4-PCD, and Ac 1,2-CTD demonstrates that the shape and chemical properties of this cavity are conserved. This is especially intriguing when one compares 3,4-PCDs and 1,2-CTDs, since residues that line this cavity in 3,4-PCD are donated by both the α and β subunit, while in 1,2-CTDs they are donated by only one subunit. This suggests that the characteristics of this cavity serve an important role in the mechanism of intradiol dioxygenases. In all three intradiol structures, a well-ordered water molecule (WAT701 in Ac 3,4-PCD) is bound in this cavity and is coordinated by $Gly13^{O}$, $Tyr16^{N}$, and $Trp400^{N\epsilon1}$. The position of WAT701 suggests that it could donate a proton to promote cleavage of the proposed peroxy intermediate.

Orville et al. (*25*, *32*) reported the presence of a secondary binding site in Pp 3,4-PCD near the apical end of the local 3-fold axes. This site was linked to the active site by a solvent-filled channel. No indication of a comparable site was found in Ac 3,4-PCD.

4-NC Complex. Crystals of Ac 3,4-PCD soaked in 4-NC resulted in an immediate color change from burgundy to purple similar to that seen in the solution complex of Ac 3,4-PCD with 4-NC. The density suggests that the binding mode of 4-NC and PCA are very similar (see Figure 3d). Like PCA, the hydroxyls of 4-NC chelate the Fe^{3+} leading to the dissociation of the axial tyrosine. The plane of the aromatic ring lies in the axial plane with the nitro group forming a similar hydrogen bond with Tyr324. However, in contrast to PCA, 4-NC binds to the Fe^{3+} more asymmetrically. While both 4-NC and PCA bind in the same orientation with the O4 in the axial position and the O3 in the equatorial position, the equatorial bond has lengthened to 2.2 Å, while the axial bond has shortened to 2.0 Å. There is also a water molecule ligated to the Fe^{3+} ($d = 2.2$ Å) in the 4-NC complex but not in the PCA complex. Another interesting feature is the absence of any waters solvating the nitro group. In the PCA complex, there are three well-ordered waters that interact with the oxygen on the carboxylate that is not hydrogen bonded to Tyr324. All other waters within 10 Å of the inhibitor are conserved between the 4-NC and PCA structures, indicating that differences between the hydration sphere of the nitro group and the carboxylate are not due to differences in the quality of the data but could result from their unique electronic states.

Cyanide Complex. Cyanide anions form very stable complexes with Fe^{3+}, and have been used extensively with ferric containing enzymes to probe coordination sites that are available to exogenous ligands. Studies of Bf 3,4-PCD

indicate that cyanide binds to 3,4-PCD in at least a two-step process (*24*). The first phase is fast ($\sim s^{-1}$), forming a high-spin complex; the second is slower ($\sim min^{-1}$) leading to a low spin complex. The two complexes have distinct optical absorption spectra with the high spin complex having a purple color ($\lambda_{max} \approx 530$ nm) and the low spin complex having a green color ($\lambda_{max} \approx 625$ nm). When crystals of Ac 3,4-PCD were incubated with 200 mM NaCN, a similar optical change was seen. Since the high-spin complex is short lived, we are unable to examine it in the time frame required by crystallographic experiments. However, the low-spin complex is stable over a long time frame and is amenable to crystallographic analysis.

$|F_o| - |F_c|$ maps indicated three positive peaks extending from the $2|F_o| - |F_c|$ density for the iron (see Figure 3e). These peaks are opposite $Tyr408^{OH}$, $His460^{N\epsilon 2}$, and $His462^{N\epsilon 2}$ and are labeled sites A, B, and C, respectively. The difference maps also showed that Tyr447 dissociates from the Fe^{3+} and forms a hydrogen bond to Tyr16 and Asp413 as it does in complexes with PCA and 4-NC. An initial model with three water molecules in these positions yielded featureless difference maps with Fe−O distances of approximately 2.6 Å. The water molecules had low thermal parameters (4−12 Å^2) compared to those of the Fe^{3+} and its other ligands (12−20 Å^2), suggesting that there might be more electron density at these positions. Orville and Lipscomb (*30*) (1989) showed that for Bf 3,4-PCD two strongly bound cyanides were retained after gel filtration of the low-spin complex and that a third binding site was available to cyanide even after PCA had chelated the Fe^{3+}. The ^{13}C broadening seen in the high-spin complex was exacerbated in the low-spin complex, suggesting that at least two molecules of cyanide may bind with a linear Fe−C−N bond geometry which would maximize the orbital overlap. Therefore, the initial model before refinement placed 3 cyanides with linear Fe−C−N geometry at a distance of 1.9 Å. During the refinement the geometry of the cyanides relative to the Fe^{3+} were not constrained.

In the final model, the cyanides all have Fe−C distances around 2.0 Å, with the Fe^{3+} having distorted octahedral geometry. The cyanides have an average thermal parameter of 15.9 Å^2, which is comparable to the other Fe^{3+} ligands. A strong electrostatic interaction is observed between CN901 (site A) and Arg457 with the cyanide N within 2.9 Å of the guanidinium NϵH2 group. CN901 also makes favorable hydrogen-bonding interactions with $Gln477^{N\epsilon 2}$ (3.1 Å) which may be partially responsible for the nonlinearity of the Fe−C−N bond seen (153°). CN902 (site B) fills the occluded space that remained after PCA or 4-NC bound. The nitrogen of cyanide makes a hydrogen bond with the backbone nitrogen of Tyr16 (3.1 Å), which appears to lead to a nonlinear Fe−C−N bond (145°). This is equivalent to the interaction seen in tertiary complex of Pp 3,4-PCD with 2-hydroxy-isonicotinic acid *N*-oxide and CN^- (*25*). CN902 also is within hydrogen-bonding distance to WAT701 (2.7 Å) only the geometry does not facilitate a strong interaction. In fact, when compared to the Ac 3,4-PCD-PCA complex CN902 appears to cause a substantial shift of WAT701 (0.75 Å) and the side chain of Trp400 (0.5 Å) away from the cyanide. This shift is not seen in the Ac 3,4-PCD native or Ac 3,4-PCD-4-NC complex, indicating that a larger ligand (i.e., CN) than WAT700 is bound at site B. The binding of cyanide to Ac 3,4-PCD appears to alter the active site hydration network seen in the native enzyme at pH 8.5. The waters closest to the Fe^{3+} shift to avoid bad contacts with the cyanides in position A and position C. This lead to having only 4 waters solvating the active site instead of 5. CN903 (site C) dissociates Tyr447 and is within hydrogen-bonding distance (2.8 Å) of a water molecule. This hydrogen bond or the close van der Waals contact of this cyanide with Tyr447 (3.2 Å) leads to the slightly bent conformation of CN903 (163°).

DISCUSSION

Ligand Shifts. While the resolution does not allow for the differentiation of small shifts in the ligand sphere from individual complexes, comparisons of several different complexes allows us to see a more accurate representation. Upon binding CN, 4-NC, or PCA, the Fe^{3+} undergoes a shift of 0.3−0.4 Å toward site A. These shifts are not seen in the native and two low pH crystal structures. The movement of the Fe^{3+} appears to cause a reproducible shift of ~0.2 Å of His462 in a parallel manner toward site A. Tyr408 shows variable movement toward site B depending on what ligand occupies that position (0.4−0.6 Å) with the largest movements occurring in the PCA and 4-NC complexes. The position of His460 does not seem to be influenced by the binding of exogenous ligands.

Structural Changes upon Fe Coordination Change. The studies presented here indicate that, upon binding a large anion in the active site, there is a reproducible shift of several residues along the $\alpha\beta$ interface of Ac 3,4-PCD. The shift appears to emanate from small structural changes within the active-site cavity and propagates through the $\alpha\beta$ interface to the outside of the protein (see Figure 6). In the native state at pH 8.5, there is a 112 Å^3 (solvent accessible volume) hydrophobic cavity which is formed by residues Tyr16, Ile19, Gly20, Ile28, Trp400, Gln401, Tyr408, Arg409, His410, Gly424, Gly425, and Cys426. One edge of this cavity is 4.9 Å away from the proposed oxygen-binding cavity, while the opposite edge is 5.6 Å away from the surface of the protein. Access to the Fe^{3+} through this cavity is hindered by a 4.5 Å × 4.7 Å × 5.1 Å triangular restriction caused by the side chains of Trp400, Tyr408, and Tyr16. Upon binding of anion in the active-site cavity there is a concerted movement of residues which results in the filling of this hydrophobic cavity. Some of the largest changes involve residues Ile19 (Cδ1-5.3 Å, Cα-3.3 Å), His18 (Cα-2.8 Å), Gln25 (Cδ-5.0 Å, Cα-4.0 Å), His410 (Nϵ2-3.7 Å, Cα-1.7 Å), and Pro411 (Cγ-4.3 Å, Cα-2.2 Å). The most dramatic change is seen for Ile19, which moves into the cavity, and lays against the triangular restriction noted above.

In all cases, the conformational change is associated with an anion binding trans to Tyr408. These changes could be attributed to shifts in the position of Pro15, which rests against the substrate and is just upstream in sequence from Ile19. However, the same change is seen in the cyanide complex even though none of the cyanides interact with Pro15. Alternatively, the dissociation of Tyr447 causes a ~0.5 Å shift in the position of Tyr16 to improve a hydrogen bond between the two tyrosines, and this may cause structural perturbations downstream at Ile19. This also most likely is not the stimulus because the conformational change does occur in the low pH studies even though Tyr447 does not

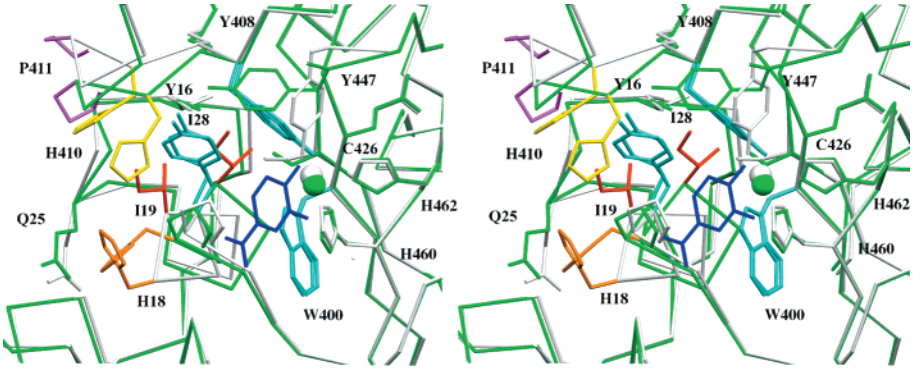

FIGURE 6: Divergent stereoview of the conformational change when small molecules bind to the Fe^{3+}. Main chain atoms of native are colored white, while those of the complex are colored green. PCA is colored blue. Residues that separate the hydrophobic pocket from the oxygen binding cavity are shown in cyan. Other residues that show significant movement are individually colored.

dissociate. In addition, Pp 3,4-PCD inhibitor complexes with small molecules that do not cause Tyr447 dissociation also show the conformational change (*32*).

The most likely trigger for this conformational change is the shift in the ligand geometry of the Fe^{3+} from trigonal bipyramidal to octahedral opening a binding site opposite Tyr408. The low pH studies suggest that binding of anions trans to Tyr408 could be induced by titrating the bound hydroxyl. A similar effect was seen in acid-alkaline transition of myoglobin in which a hydroxyl bound to the sixth coordinate spot of the heme can be titrated off with an apparent pK_a of 7.5 (*50*−*53*). Thus, it is reasonable that shifting the pH from 8.5 to 5.75 could protonate the hydroxyl (consistent with an increase in d(Fe−OH) from 1.9 to 2.3 Å), placing a net positive charge at the Fe^{3+} center. This positive charge is destabilizing due to the proximity of Arg457. The binding of a sulfate would then neutralize both of these positive charges. Movement of Tyr408 (described previously) upon forming an Fe^{3+} with more octahedral character could have direct effects on the position of His410 and lead to the conformational change.

One hypothesis as to the function of the structural rearrangements would be to facilitate the reaction of oxygen with the substrate. This could be accomplished in one of three ways. (1) The general flexibility of the region, and transition from one conformation to another in a general fashion improves the diffusion rate of oxygen. (2) The hydrophobic cavity is the loading point for oxygen, which upon the binding of substrate to Fe^{3+} is pushed into the active site by Ile19. (3) The lower flexibility after binding substrate (closed conformation) ensures that the intermediates in the reaction (i.e., OH^-) do not have access to bulk solvent.

It has recently been proposed that there is a specific oxygen pathway to the heme group in cytochrome C oxidase (*54*). Molecular dynamics simulations of oxygen diffusion through the protein indicates a pathway starting at a hydrophobic cavity leading to a restricted opening between an aromatic residue and a tryptophan (*55*). In these simulations, the oxygen molecules showed a distinct preference for hydrophobic cavities. We argue against a specific pathway for oxygen based on the evidence of several O_2 tryptophan quenching studies that indicate that proteins do not present a formidable barrier to O_2 due to its small size and apolar nature (*56*, *57*). Normal diffusion of O_2 is more than adequate to react with substrate during the reaction scheme. In addition, while the proposed pathway from the Fe^{3+} to the hydrophobic cavity to the exterior of protein is 15 Å in length, oxygen could instead travel along the substrate cavity and be only 6 Å from the Fe^{3+}. We also argue against there being any need to further restrict the active site in order to retain the oxygen intermediates. While studies of slow substrates such as pyrogallol have shown that some proportion of the oxygen intermediate is able to react with solvent (*58*), the reaction of oxygen with PCA most likely occurs too rapidly for the hydroxide intermediate to diffuse away from the Fe^{3+}.

A more likely hypothesis is one in which the conformational change is used to increase the affinity of the enzyme for substrate and to decrease the affinity of the enzyme for product. There is no product inhibition in this enzyme system since once the product leaves the active site it is free to undergo a cis−trans isomerization and is no longer constrained to be planar. However, product release from the active site is the slow step in the reaction scheme. The active sites of Ac 3,4-PCD and Pp 3,4-PCD have been shown to have a preponderance of positive charge in and around the active site despite having a large overall negative charge. This has been postulated to function as a funnel for the negatively charged substrate (PCA) to attract it to the active site. While this would facilitate the interaction of substrate with the Fe^{3+}, it also inhibits product release since the product is even more electronegatively charged then the substrate (−3 vs −2). In addition, it is known that the Fe^{3+} of 3,4-PCDs binds various compounds through their carboxylates (*48*). One way to overcome this is to lower the affinity of the Fe^{3+} for the product in relation to substrate through steric constraints. We do not know the transition pathway from the bound conformation to unbound conformation, but this could very well involve movements of residues which interact with the substrate (i.e., Pro15, Tyr16, Tyr447). While the trigger of the movements would be binding of the O4 group of substrate trans to 408, this would be correlated with the dissociation of Tyr447, and movements of Pro15 and Tyr16, which could lead to improved binding of substrate. On the other hand, once the aromatic ring is cleaved, it loses its planar character. This could be the signal to reverse the conformational changes. Tyr447 swings back onto the Fe^{3+} potentially leaving product with one carboxylate bound trans to Tyr408. The residues along the α/β interface return to the unbound state which promotes rebinding of hydroxyl and creation of trigonal planar Fe^{3+}, thereby lowering the affinity of product. Ac 3,4-PCD shows a maximum rate at pH 8.5−

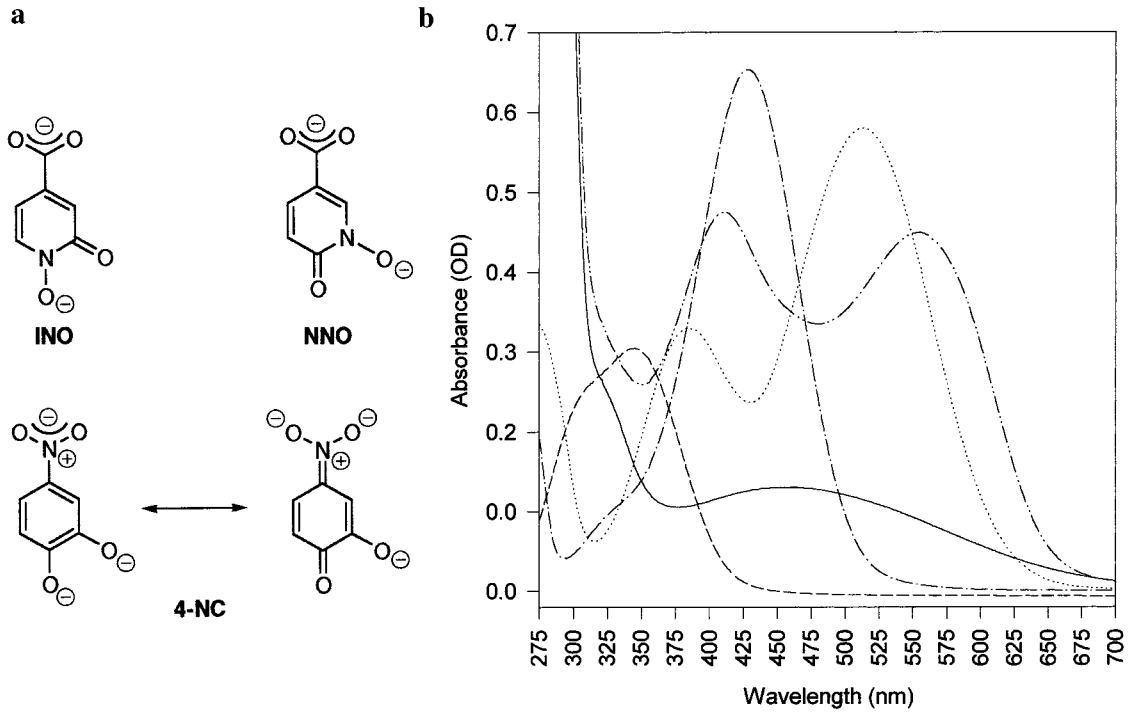

FIGURE 7: (a) Ketonized tautomers of INO and NNO, and a potential resonance structure of 4-NC when bound to Ac 3,4-PCD. (b) Optical spectrum of 40 μM 4-NC at pH 4.0 (− − −), pH 7.5 (−•−•−), pH 12.0 (•••), pH 7.5 + 40 μM Ac 3,4-PCD active sites (−••−••−), and 40 μM active sites Ac 3,4-PCD (solid line).

9.0 with an apparent molecular pK_a of ~7.75. The binding of anions (i.e., carboxylates) increases as the pH is lowered and correlates with the molecular pK_a of the enzyme (data not shown). If product release remains the slow step throughout this pH range, then the apparent molecular pK_a could be attributed to the hydroxyl group bound to the Fe^{3+} or the protonation of a group in the α/β interface.

Binding of CNs. While the number of cyanides and their orientation could not be unambiguously determined due to the resolution of the data, previous kinetic and crystallographic data suggest that cyanide is bound in all exogenous ligand sites (A−C). (1) The binding reaction of cyanide to Bf 3,4-PCD is biphasic and each phase is inhibited by PCA (*29*). This suggests that sites A and C can bind cyanide since these are the sites occupied by PCA. (2) Electron density for cyanide was observed at position B when enzyme was incubated with a transition-state analogue and 200 mM NaCN, indicating that site B can bind cyanide when site A and site C are occupied by other exogenous ligands (*25*). (3) Three cyanides are proposed to bind to the ferric Fe^{3+} within the C-terminal lobe of transferrin. This complex gives a low-spin species with similar EPR signals (g = 2.34, 2.15, 1.92) when compared to the 3,4-PCD low spin complex (g = 2.43, 2.21, 1.89) (*59*). (4) The movement of residues and solvent molecules in the Ac 3,4-PCD-CN complex and the formation of several favorable hydrogen bonds are compatible with three cyanides. (5) All three sites have similar density features consistent with three cyanides bound. (6) Finally, neither the high-spin CN complex nor the low-spin CN complex exhibits any ^{17}O water broadening in their EPR signals, suggesting that water is not a ligand in either complex.

All previously solved complexes of 3,4-PCD result in a neutral Fe^{3+} center. The short CN−Fe distances suggests that cyanide is coordinated as CN^-. Since the distance between Fe and $Tyr408^{OH}$ is unchanged from native, Tyr408 probably remains deprotonated. Thus, the overall net charge of the Fe^{3+} center may be negative. The characteristically tight binding of CN^- may overrule the tendencies of the enzyme to remain neutral. In studies with Bf 3,4-PCD, only two cyanides remained bound after gel filtration (*30*), indicating that one of the three cyanides may dissociate at low concentrations of CN^-, restoring charge neutrality at the Fe^{3+}.

Binding of 4-NC. Nitroaromatic compounds are prevalent in the environment because of their use as synthetic intermediates, dyes, pesticides, and explosives. To date no degradative pathway has been isolated which utilizes these compounds through a dioxygenase catalyzed cleavage of a nitro substituted ring. The only degradative pathway of a nitroaromatic which entails the use of a dioxygenase involves the reduction of nitrobenzene to 2-aminophenol which is subsequently cleaved by an extradiol dioxygenase (*60*). Since 4-NC is isosteric with PCA, it is interesting that 4-NC is not cleaved by 3,4-PCD. The nature of binding of 4-NC to 3,4-PCD has been the subject of debate. Its tight binding constant (K_i = 0.9 μM) and its action as a competitive inhibitor suggest it binds at the active site. The spectrum of the 4-NC complex with Pp 3,4-PCD is very stable, remaining unchanged after incubation at 4 °C for over a year, and (*26*) the enzyme was still able to turn over substrate after this period. When 4-NC is complexed with Pp 3,4-PCD, the EPR spectrum drastically changes lending support that the Fe^{3+} ligation sphere is changed by 4-NC (*26*). The resonance Raman spectrum of Pp 3,4-PCD complexed with 4-NC is similar to that of the dianionic form of 4-NC alone (*48*), but the spectrum was missing the usual features typical seen with the binding of a catecholate to Fe^{3+}. It was proposed that 4-NC might be binding to the Fe^{3+} as the O4 ketonized tautomer or might bind in a backward orientation with the phenolate oxygens interacting with the carboxylate binding

site for PCA ($Tyr324^{OH}$) (*48*, *61*). The data presented here indicates that the inability of 3,4-PCDs to turnover 4-NC is not due to incorrect binding. It is apparent that the inductive withdrawal of electron density from the aromatic ring by the nitro group deactivates the ring toward reactions with electrophiles. This is especially true at the carbon para to the nitro group (C4) which is the proposed site of interaction with oxygen.

The transition-state analogues INO and NNO are proposed to mimic the ketonized tautomers of PCA at O3 and O4, respectively. Previous studies have shown that INO (K_d = 0.06 μM) and NNO (K_d = 0.20 μM) are strong inhibitors of the enzyme (*24*). Crystallographic studies of INO and NNO in complex with Pp 3,4-PCD indicate that they form chelated complexes with similar Fe^{3+} ligation distances as seen in the PCA-Pp 3,4-PCD complex (*25*). Figure 7a shows that 4-NC can form a similar ketonized structure. Two forms of structural evidence support that 4-NC has significant ketonized character when chelated to Ac 3,4-PCD. (1) Binding of an OH/OH_2 opposite to His460 indicates the Fe^{3+} is electron deficient. In both the INO and NNO complexes a similar water was seen bound at this position. (2) The loss of several coordinating water molecules suggests that the oxygen of the nitro group has different electron character than the carboxylate oxygens of PCA.

The protonation state of PCA bound to 3,4-PCD cannot be determined through absorption spectroscopy since the protein absorbs in the same region. However, the protonation state of 4-NC can be used since its absorption maximums are at much longer wavelengths. When a neutral solution of 4-NC is mixed with a stoichiometric amount of Ac 3,4-PCD, the absorption spectra resembles the spectrum of the 4-NC dianion displaced to a longer wavelength (see Figure 7b). This is comparable to the spectra seen of 4-NC titrated with Pp 3,4-PCD. (*26*). The binding of PCA as a dianion is an important feature of the proposed mechanism. The similarity in the binding orientation of PCA and 4-NC suggests that PCA also binds as a dianion.

SUMMARY

High-resolution crystallographic studies of Pp 3,4-PCD and Ac 1,2-CTD have indicated several important features of enzymes which exhibit intradiol dioxygenase activity: (1) high-affinity binding of substrates in a chelated complex to the Fe^{3+}, (2) ligand dissociation upon binding substrate, (3) positioning of a basic group near C4 of substrate within a low dielectric cavity, and (4) sequestering of a small molecule binding cavity away from bulk solvent and adjacent to the Fe^{3+} and C4 carbons of substrate. These studies have been enhanced by the structural studies of Ac 3,4-PCD reported here. Complexes with PCA and 4-NC demonstrate a similar chelated binding as seen with Pp 3,4-PCD substrate and inhibitor complexes. Residues proposed to be critical to positioning of substrate are in similar positions and conformations. Tyr447 was seen to dissociate upon binding 4-NC, PCA or cyanide. The crystal structure of the strong inhibitor 4-NC is consistent with the studies of Pp 3,4-PCD binding of INO and NNO demonstrating the enzymes preference for a dianionic ketonized transition state. In both the PCA and 4-NC complexes, a small molecule binding cavity is conserved and sequestered from bulk solvent. The proportions of the cavity are similar to what would be needed to bind oxygen and would allow direct interaction with the C4 carbon of substrate. Crystallographic analysis of the low spin cyanide complex suggests that the enzyme is capable of binding three exogenous ligands with distorted octahedral geometry.

ACKNOWLEDGMENT

The authors wish to acknowledge the Minnesota Supercomputer Institute for providing computational resources. The authors wish to thank Dr. John Lipscomb and Dr. Allen Orville for helpful discussions.

REFERENCES

1. Alexander, M. (1981) *Science 211*, 132−8.
2. Armstrong, S. M., and Patel, T. R. (1994) *J. Basic Microbiol. 34*, 123−35.
3. Gibson, D. T., and Subramanian, V. (1984) in *Microbial Degradation of Aromatic Hydrocarbons* (Gibson, D. T., Ed.) pp 181−252, Marcel Dekker, New York.
4. Dagley, S. (1977) *Surv. Progr. Chem. 8*, 121−70.
5. Dagley, S. (1978) in *The Bacteria* (Ornston, L. N., and Sokatch, J. R., Eds.) pp 305−88, Academic Press, Inc., New York.
6. Stanier, R. Y., and Ingraham, J. L. (1954) *J. Biol. Chem. 210*, 799−808.
7. Miller, M. A., and Lipscomb, J. D. (1996) *J. Biol. Chem. 271*, 5524−35.
8. Que, L. Jr., Lipscomb, J. D., Münck, E., and Wood, J. M. (1977) *Biochim. Biophys. Acta 485*, 60−74.
9. Han, S., Eltis, L. D., Timmis, K. N., Muchmore, S. W., and Bolin, J. T. (1995) *Science 270*, 976−80.
10. Senda, T., Sugiyama, K., Narita, H., Yamamoto, T., Kimbara, K., Fukuda, M., Sato, M., Yano, K., and Mitsui, Y. (1996) *J. Mol. Biol. 255*, 735−52.
11. Kita, A., Kita., S.-i., Fujisawa, I., Inaka, K., Ishida, T., Horiike, K., Nozaki, M., and Miki, K. (1999) *Structure 7*, 25−34.
12. Sugimoto, K., Senda, T., Aoshima, H., Masai, E., Fukuda, M., and Mitsui, Y. (1999) *Stuct. Folding Des. 7*, 953−65.
13. Ohlendorf, D. H., Lipscomb, J. D., and Weber, P. C. (1988) *Nature 336*, 403−5.
14. Ohlendorf, D. H., Orville, A. M., and Lipscomb, J. D. (1994) *J. Mol. Biol. 244*, 586−608.
15. Vetting, M. W., and Ohlendorf, D. H. (2000) *Stuct. Folding Des.* 429−40.
16. Que, L., Jr. (1983) *Adv. Inorg. Biochem. 5*, 167−99.
17. Lipscomb, J. D., Howard, J. B., and Wood, J. M. (1982) *Oxygenases and Related Redox Systems*, pp 483−507.
18. Hammer, A., Stolz, A., and Knackmuss, H. (1996) *Arch. Microbiol. 166*, 92−100.
19. Lipscomb, J. D., and Orville, A. M. (1992) in *Metal Ions in Biological Systems* (Sigel, H., and Sigel, A., Eds.), Marcel Dekker, Inc., New York.
20. Vetting, M. W., Earhart, C. A., and Ohlendorf, D. H. (1994) *J. Mol. Biol. 236*, 372−3.
21. Gerischer, U., and Ornston, L. N. (1995) *J. Bacteriol. 177*, 1336−47.
22. D'Argenio, D. A., Vetting, M. W., Ohlendorf, D. H., and Ornston, L. N. (1999) *J Bacteriol 181*, 6478−87.
23. Juni, E., and Janik, A. (1969) *J. Bacteriol. 98*, 281−8.
24. Whittaker, J. W., and Lipscomb, J. D. (1984) *J. Biol. Chem. 259*, 4476−86.
25. Orville, A. M., Lipscomb, J. D., and Ohlendorf, D. H. (1997) *Biochemistry 36*, 10052−10066.
26. Tyson, C. A. (1975) *J. Biol. Chem. 250*, 1765−70.
27. Whiting, A. K., Boldt, Y. R., Hendrich, M. P., Wackett, L. P., and Que, L., Jr. (1996) *Biochemistry 35*, 160−70.
28. Que, L., Jr., Widom, J., and Crawford, R. L. (1981) *J. Biol. Chem. 256*, 10941−4.
29. Whittaker, J. W., and Lipscomb, J. D. (1984) *J. Biol. Chem. 259*, 4487−95.

30. Orville, A. M., and Lipscomb, J. D. (1989) *J. Biol. Chem. 264*, 8791−801.
31. Orville, A. M., and Lipscomb, J. D. (1997) *Biochemistry 36*, 14044−55.
32. Orville, A. M., Elango, N., Lipscomb, J. D., and Ohlendorf, D. H. (1997) *Biochemistry 36*, 10039−10051.
33. Howard, A. J., G. L., G., Finzel, B. C., Poulos, T. L., Ohlendorf, D. H., and Salemme, F. R. (1987) *J. Appl. Crystallogr. 20*, 383−7.
34. Brünger, A. T. (1992) *Acta Crystallogr., Sect. D 49*, 24−46.
35. Fujisawa, H., and Hayaishi, O. (1968) *J. Biol. Chem. 243*, 2673−81.
36. Hou, C. T., Lillard, M. O., and Schwartz, R. D. (1976) *Biochemistry 15*, 582−8.
37. Doten, R. C., Ngai, K. L., Mitchell, D. J., and Ornston, L. N. (1987) *J. Bacteriol. 169*, 3168−74.
38. Fujiwara, M., and Nozaki, M. (1973) *Biochim. Biophys. Acta 327*, 306−12.
39. Brünger, A. T. (1993) *X-PLOR Version 3.1 Manual*, Yale University, New Haven, CT.
40. Jones, T. A., Zou, J. Y., Cowan, S. W., and Kjeldgaard, M. (1991) *Acta Crystallogr,, Sect. A 47*, 110−119.
41. Brünger, A. T., Adams, P. D., Clore, G. M., DeLano, W. L., Gros, P., Grosse-Kunstleve, R. W., Jiang, J. S., Kuszewski, J., Nilges, M., Pannu, N. S., Read, R. J., Rice, L. M., Simonson, T., and Warren, G. L. (1998) *Acta Crystallogr., Sect. D 54*, 905−21.
42. Getzoff, E. D., Cabelli, D. E., Fisher, C. L., Parge, H. E., Viezzoli, M. S., Banci, L., and Hallewell, R. A. (1992) *Nature 358*, 347−51.
43. Lindbladh, C., Rault, M., Hagglund, C., Small, W. C., Mosbach, K., Bulow, L., Evans, C., and Srere, P. A. (1994) *Biochemistry 33*, 11692−8.
44. Kohlmiller, N. A., and Howard, J. B. (1979) *J. Biol. Chem. 254*, 7309−15.
45. Iwaki, M., Kagamiyama, H., and Nozaki, M. (1981) *Arch. Biochem. Biophys. 210*, 210−23.
46. Frazee, R. W., Livingston, D. M., LaPorte, D. C., and Lipscomb, J. D. (1993) *J. Bacteriol. 175*, 6194−202.
47. Hartnett, C., Neidle, E. L., Ngai, K. L., and Ornston, L. N. (1990) *J. Bacteriol. 172*, 956−66.
48. Que, L., Jr., and Epstein, R. M. (1981) *Biochemistry 20*, 2545−9.
49. Frazee, R. W., Orville, A. M., Dolbeare, K. B., Yu, H., Ohlendorf, D. H., and Lipscomb, J. D. (1998) *Biochemistry 37*, 2131−44.
50. Ascenzi, P., Giacometti, G. M., Antonini, E., Rotilio, G., and Brunori, M. (1981) *J. Biol. Chem. 256*, 5383−6.
51. Giacometti, G. M., Ascenzi, P., Bolognesi, M., and Brunori, M. (1981) *J. Mol. Biol. 146*, 363−74.
52. Giacometti, G. M., Ascenzi, P., Brunori, M., Rigatti, G., Giacometti, G., and Bolognesi, M. (1981) *J. Mol. Biol. 151*, 315−9.
53. Conti, E., Moser, C., Rizzi, M., Mattevi, A., Lionetti, C., Coda, A., Ascenzi, P., Brunori, M., and Bolognesi, M. (1993) *J. Mol. Biol. 233*, 498−508.
54. Tsukihara, T., Aoyama, H., Yamashita, E., Tomizaki, T., Yamaguchi, H., Shinzawa-Itoh, K., Nakashima, R., Yaono, R., and Yoshikawa, S. (1996) *Science 272*, 1136−44.
55. Hofacker, I., and Schulten, K. (1998) *Proteins 30*, 100−7.
56. Lakowicz, J. R., and Weber, G. (1973) *Biochemistry 12*, 4161−70.
57. Lakowicz, J. R., and Weber, G. (1973) *Biochemistry 12*, 4171−9.
58. Saeki, Y., Nozaki, M., and Senoh, S. (1980) *J. Biol. Chem. 255*, 8465−71.
59. Swope, S. K., Chasteen, N. D., Weber, K. E., Harris, D. C. (1988) *J. Am. Chem. Soc. 110*, 3835−40.
60. Park, H. S., and Kim, H. S. (2000) *J. Bacteriol. 182*, 573−80.
61. Walsh, T. A., and Ballou, D. P. (1983) *J. Biol. Chem. 258*, 14413−21.
62. Kraulis, P. J. (1991) *J. Appl. Crystallogr. 24*, 946−50.
63. Jones, T. A. (1978) *J. Appl. Crystallogr. 11*, 268−272.
64. Kleywegt, G. J., and Jones, T. A. (1994) *Acta Crystallogr., Sect. D 50*, 178−185.
65. Evans, S. V. (1993) *J. Mol. Graph. 11*, 134−8, 127−8.

BI000151E